Protein-Directed Assembly of Arbitrary Three-Dimensional Nanoporous Silica Architectures

Constantine Y. Khripin,[‡] Denis Pristinski,[§] Darren R. Dunphy,[‡] C. Jeffrey Brinker,[†,‡] and Bryan Kaehr*[,†]

[†]Advanced Materials Laboratory, Sandia National Laboratories, Albuquerque, New Mexico, United States, [‡]NSF/UNM Center for Micro-Engineered Materials, Departments of Chemical and Nuclear Engineering and Molecular Genetics and Microbiology, University of New Mexico, Albuquerque, New Mexico, United States, and [§]Polymers Division, National Institute of Standards and Technology, Gaithersburg, Maryland, United States

ABSTRACT Through precise control of nanoscale building blocks, such as proteins and polyamines, silica condensing microorganisms are able to create intricate mineral structures displaying hierarchical features from nano- to millimeter-length scales. The creation of artificial structures of similar characteristics is facilitated through biomimetic approaches, for instance, by first creating a bioscaffold comprised of silica condensing moieties which, in turn, govern silica deposition into three-dimensional (3D) structures. In this work, we demonstrate a protein-directed approach to template silica into true arbitrary 3D architectures by employing cross-linked protein hydrogels to controllably direct silica condensation. Protein hydrogels are fabricated using multiphoton lithography, which enables user-defined control over template features in three dimensions. Silica deposition, under acidic conditions, proceeds throughout protein hydrogel templates *via* flocculation of silica nanoparticles by protein molecules, as indicated by dynamic light scattering (DLS) and time-dependent measurements of elastic modulus. Following silica deposition, the protein template can be removed using mild thermal processing yielding high surface area (625 m^2/g) porous silica replicas that do not undergo significant volume change compared to the starting template. We demonstrate the capabilities of this approach to create bioinspired silica microstructures displaying hierarchical features over broad length scales and the infiltration/functionalization capabilities of the nanoporous silica matrix by laser printing a 3D gold image within a 3D silica matrix. This work provides a foundation to potentially understand and mimic biogenic silica condensation under the constraints of user-defined biotemplates and further should enable a wide range of complex inorganic architectures to be explored using silica transformational chemistries, for instance silica to silicon, as demonstrated herein.

KEYWORDS: biomimetic synthesis · biomineralization · diatom · multiphoton fabrication · silica · silicon

The biomimetic approach to materials design and fabrication has provided material scientists and chemists an inspirational and accessible framework within which to explore the lessons offered by evolutionarily tested, complex materials. Silica condensing microorganisms, such as diatoms, offer a prime case study for biological design and construction strategies. They are consistently revered for their ability to construct intricate architectures with hierarchical features across milli- to nanometer-length scales. The desire to both understand and exploit these material processing capabilities has been a driving force for considerable scientific effort worldwide.[1−10] Though these efforts have revealed some of the mechanisms of biogenic silica formation,[1] anthropogenic synthesis and assembly of silica into programmed three-dimensional (3D) architectures remains a challenge. Thus, an increasingly common route to take advantage of diatoms' ability to build inorganic microarchitectures has been to employ the biogenic silica templates (diatom frustules) as starting materials for subsequent chemical modification[4] or replica molding.[11,12] This route has led to pioneering templating strategies and to the ability to chemically transform silica to generate, for instance, nonsilica-based oxides,[13−17] semiconductors,[18] polymers,[12,19,20] carbon,[21,22] metals,[11,23,24] and metal chalcogenides,[25] all of which inherit structural features of the initial biological template.

Ultimately, the ability to wield control over all aspects of the synthesis—from template design and fabrication to subsequent functionalization—will expand the pool of applications and facilitate device integration of silica-templated 3D materials. Crucial toward this goal is the development of strategies to assemble or otherwise template silica into desired architectures. Furthermore, by developing lithographic approaches, nanostructured patterns can be achieved over much larger length scales, not limited to the dimensions of diatoms. Toward the design of lithographically definable silica templating materials, the Yang group has shown that photolithographically patterned hydrogels functionalized with polyethyleneimine could template 2D patterns of silica nanoparticles following calcination of the hydrogel template.[26] This group also has demonstrated the fabrication of 3D organosilicates using interferometric lithography of photoresists

*Address correspondence to bjkaehr@sandia.gov.

Received for review November 22, 2010 and accepted December 26, 2010.

Published online 10.1021/nn1031774

functionalized with oligomeric silsesquioxanes.[27] The resulting structures could be thermally converted to silica at 400 °C. These studies provide promising steps forward in the design of catalytic templates, but the lithographic procedures lack true three-dimensional control over template architectures.

The Lewis group has demonstrated the use of 3D polymer scaffolds, enriched with polyamines and assembled using a layer by layer direct-ink writing approach, to template silica into diatom-like objects.[28] Preservation of the silica structure required thermal pretreatment of the scaffold followed by sequential immersion in silica acid and phosphate buffer over a 2 day period. The ink template could be removed at high temperature (1000 °C), yielding a partially sintered silica replica with a two-fold decrease in size *versus* the starting template. This work was first to demonstrate the possibility of creating biomimetic silica morphologies. However, though direct-ink writing enables construction of 3D scaffolds, true arbitrary control is not generally feasible due to the lack of rigidity of inks, requiring free-standing structures to be held by lattice-type supports.

Other groups have used multiphoton lithography, which offers 3D control over microstructure features, to cure structures from photopolymer resins and photoresists, such as SU-8. These structures have then been used to template a wide range of other materials, including metals and metal oxides[29] *via* liquid-phase, chemical vapor, or atomic layer deposition approaches resulting in coated structures that can be transformed to, for instance, inverse replicas through decomposition of the polymer support.[30] However, these coating approaches often employ multiple clean room processing steps, are intrinsically limited to surface functionalization, and can generate distortions in the final structure due to coating heterogeneities or during template removal.

Alternative routes to template silica in 3D are offered by microorganisms. Peptides and proteins have been identified as key elements in biogenic silica formation,[1,7−9,31,32] and it has been proposed that silicagenic organisms use 3D protein scaffolds to guide silica condensation.[1,7,10] In addition to these native molecules, other proteins, such as bovine serum albumin (BSA) and lysozyme,[33,34] gelatin,[35] trypsin, and proteinase K,[36] have been shown to direct silica condensation under solution conditions where, in general, the net charge of the protein is positive (*i.e.*, $pH_{(soln)} < pI_{(prot)}$) and the soluble silica species are negative (pH > 4). Electrostatic attraction and hydrogen bonding between the protein and the soluble silicic acid species have been proposed as mechanisms for explaining silica condensation on the protein surface. In general, these strategies have enabled the synthesis of silica particles and monoliths under chemically mild reaction conditions.[8,9,34,35,37] However, to date, the controlled generation of more elaborate silica architectures using protein-directed approaches has not been reported.

In this work, we demonstrate a protein-directed approach to template nanoporous silica frameworks into arbitrary 3D architectures by employing cross-linked protein hydrogels to controllably direct silica condensation. Protein hydrogels are fabricated using multiphoton lithography to specify template features in three dimensions. Deposition of silica produces a mechanically stable, interpenetrating silica framework. Thus, the protein template can be removed using mild (nonsintering) thermal processing to yield nanoporous, high surface area silica replicas that do not undergo significant volume changes in comparison to the starting template. We demonstrate the capabilities of this approach to create bioinspired silica microstructures that display hierarchical features over broad length scales and the accessibility of the nanoporous framework by multiphoton laser printing of metallic gold within a silica microstructure *via* photoreduction of soluble metal ions.

RESULTS AND DISCUSSION

As depicted in Figure 1a, templates comprised of photocross-linked protein hydrogels were fabricated using mask-directed multiphoton lithography (MDML), an intrinsically 3D direct-write technique for rapid microprototyping of user-defined architectures.[38,39] In this procedure, a pulsed laser is scanned across a digital mirror device (DMD) displaying a sequence of 2D image slices of a 3D object, and the reflection is focused into a protein/photosensitizer solution. Cross-linking of oxidizable amino acid residues occurs within femtoliter excitation volumes (voxels) *via* multiphoton excitation of the photosensitizer.[40] Coordinating the display of image slices to axial steps of the laser focus within the reagent solution produces a 3D protein hydrogel microstructure. Here, hydrogel block-shaped microcantilevers (structures that enable the elastic modulus to be easily monitored by atomic force microscopy; AFM)[41] comprised of photocross-linked proteins were employed as templates for subsequent chemical transformation to silica and further to silicon (Figure 1b). The hydrogel properties of MDML protein matrices have been previously characterized.[41,42] Importantly, hydrated protein templates allow soluble silica precursors (*i.e.*, monomers/polymers/particles of silicic acid) to diffuse and react throughout the entirety of the 3D protein matrix.

Using tetramethyl orthosilicate (TMOS) hydrolyzed in 1 mM HCl as the source of silicic acid, silica condensation was investigated on structures made from several proteins (lysozyme, avidin, and BSA) over a range of solution conditions (pH 3, 7, 9; with and without 150 mM salts present) using AFM, thermal treatment, and elemental analyses. Condensation was not observed for protein hydrogels in pH 9 solutions.

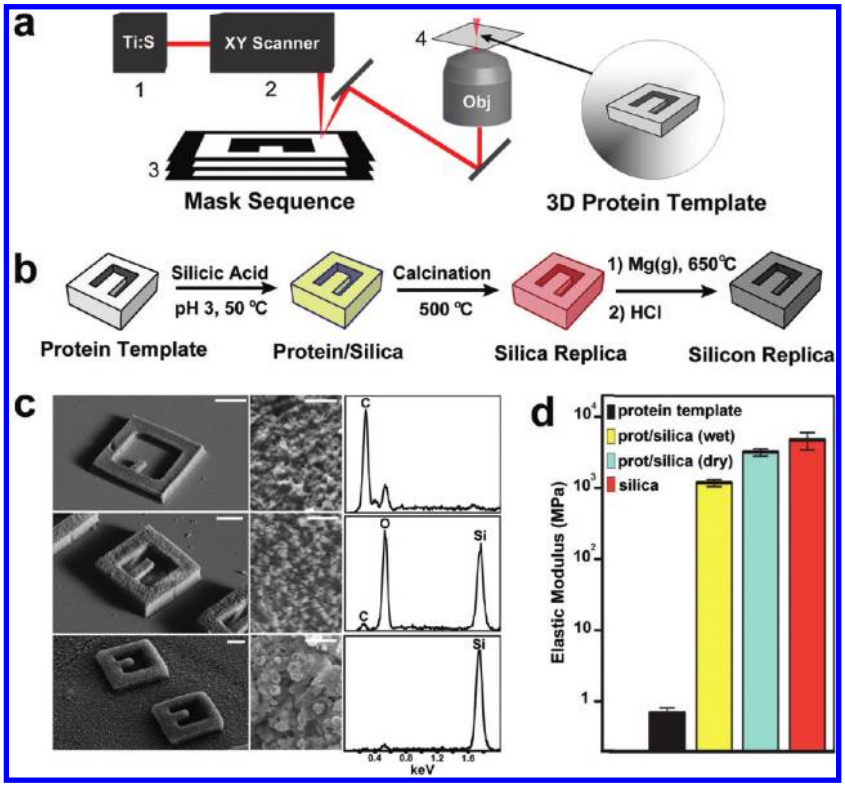

Figure 1. 3D protein microstructures template silica deposition. (a) Simplified schematic of protein template fabrication (see ref 39). The output of a mode-locked Ti:S laser (1) is raster scanned (2) across a horizontally sectioned sequence of 2D reflectance images (3, displayed by a digital micromirror device) describing a 3D object. The reflectance off the mask is focused into a protein fabrication solution to generate a 3D microstructure upon a substrate (4). (b) Protein microstructures (light gray) template silica condensation to form protein/silica hybrid structures (yellow). Calcination at 500 °C removes the protein component leaving a silica replica (red) that is converted to silicon *via* magnesiothermal reduction of silica (dark gray). (c) SEM images of protein, silica, and silicon microcantilevers (left panels, top to bottom respectively; scale bars, 10 μm), higher resolution surface topography (middle panels, scale bars 1 μm), and corresponding EDS spectra (right panels show relative intensity). (d) Elastic modulus of protein, protein/silica (wet and dry), and silica materials measured on corresponding cantilevers with an AFM and analyzed using a cantilever beam model (see ref 41).

At pH 7, silicification and desilicification were observed (Supporting Information, Figure S1); however, the silica sol would often gel under short time scales (hours) prohibiting diffusion of silica precursors throughout the protein template. By adjusting the sol to a pH of greater stability (pH 2−3),[43] silica condensation was confined to the protein templates, proceeding over a course of ~5 days (Supporting Information, Figure S2). Using mildly elevated temperatures (50 °C) to enhance both the diffusion rates of silica precursors and the rate of condensation,[43] protein-directed silica condensation was complete in ~16 h (Supporting Information, Figure S2). The protein templates were removed *via* calcination at 500 °C for 3 h to yield nearly identical silica replicas (Figure 2) with contiguous structure throughout the matrix (Supporting Information, Figure S3). Replication fidelity (or, at minimum, a precise understanding of photoresist shrinking behavior) is crucial for all lithographic processes. As an example, protein-based traps have been used to capture motile bacteria from the surrounding environment in order to develop cell-powered microfluidics[44] as well as study bacterial group behavior[45] (*e.g.*, quorum sensing). Figure 2 demonstrates high-fidelity replication, from protein to silica, of a bacterial trap. This provides opportunities to precisely interface cells to a broad range of `breathable' (*i.e.*, porous) inorganic 3D materials without the need to modify template design (*e.g.*, aperture dimensions, Figure 2b and c) in order to accommodate shrinking or swelling effects inherent to most other lithographic procedures.

Nitrogen adsorption measurements on silica templated *via* single-photon cross-linked BSA gels indicated a high specific surface area of 625 $m^2\ g^{-1}$ (Brunauer−Emmett−Teller, BET) with a broad pore width distribution varying from 5 to ~25 nm (Supporting Information, Figure S4). Template removal was verified using energy dispersive spectroscopy (EDS; Figure 1c) and Fourier transform infrared spectroscopy (FTIR; Supporting Information, Figure S5). FTIR measurements indicate that the protein template does not change significantly following silica deposition, as indicated by amide (protein signature) peak retention in the composite spectra (Supporting Information, Figure S5). We note that proteins with a range of isoelectric points (*e.g.*, lysozyme, avidin, and BSA) all formed

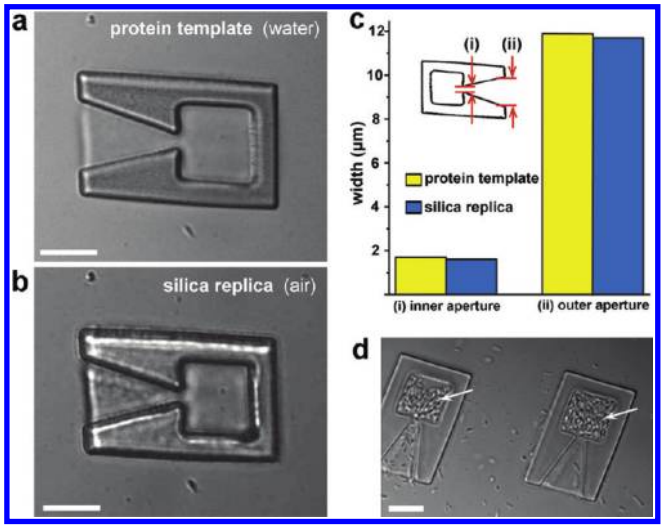

Figure 2. High-fidelity replication of microstructures. (a) A microstructure designed to trap motile bacteria (see refs 44 and 45) comprised of photo-cross-linked BSA, (a), templates a silica replica, (b). (c) The inner and outer microchamber apertures of the protein structure and silica replica are compared and show near identical widths. (d) Motile bacteria are captured and confined in the replicas, dividing to form high-density cell colonies (arrows) in porous silica microchambers over 24 h. Scale bars for (a, b, and d) are 10 μm.

protein/silica composites under these conditions. Unless otherwise noted, BSA-templated structures were employed for further characterization.

The process of silica condensation on protein templates was monitored *in situ* by periodically measuring the modulus of the protein microcantilever using an AFM method described previously by our group.[41] The elastic modulus of microstructures increased from 0.1 to 3 MPa for protein cantilevers to *ca*. 5 GPa following calcination (Figure 1d). This modulus value was not dependent on initial stiffness (a function of the density/degree of cross-linking)[42] of the protein template (Supporting Information, Figure S6). Further, silica replicas were subjected to magnesiothermal reduction[18] to form silicon replicas (Figure 1a and b lower panels). This process flow—from protein hydrogel template, to silica, to silicon—demonstrates a feasible route to microfabricate a wide-range of 3D inorganic materials using the myriad of transformational chemistries that have been developed for diatom frustules as starting materials.[4]

Protein template fabrication using MDML enables image data sets to be rapidly translated into 3D microobjects,[39] allowing elaborate biological features to be replicated. To demonstrate the capabilities of protein-directed silica assembly to template complex silica structures, diatom/radiolaria image sets were used to direct fabrication of a BSA template (Figure 3). Figure 3a shows images of diatoms (top left panels) that were used to direct fabrication of protein templates (top right panel), subsequently converted to silica replicas (bottom panel). Hollow, free-standing 3D silica structures, such as radiolaria-like frustules (Figure 3b), can be fabricated using these procedures without requiring mechanical supports. These diatom replicas exhibit hierarchical features across tens of micrometer- to nanometer-length scales (Figure 3c). SEM (Figure 3c, bottom left panel) and TEM images (Supporting Information, Figure S5) show a rough, amorphous surface comprised of particles on the order of ~20−60 nm in diameter; AFM phase images (Figure 3c, bottom right panel; Supporting Information, Figure S7) show the surface of the particles is composed of approximately uniform features (coalesced primary particles) on the order of tens of nanometers in size (measured size of smallest discernible particles 16 ± 3 nm from SEM images and 16 ± 4 nm from AFM images).

These features are consistent with flocculation and further coarsening (*i.e.*, dissolution and reprecipitation driven by differences in solubility between surfaces of different curvature) of primary silica particles known to form under acidic pH in supersaturated solutions of silicic acid (>2 mM, pH 2−7, room temperature).[43] Throughout the hydrogel matrix, photo-cross-linked BSA molecules act as flocculating agents of silica precursors and particles. We observed silicification at pH 2, where the silica is uncharged,[33,43] suggesting that the nature of the protein−silica interaction is largely mediated by hydrogen bonding *versus* electrostatic interactions, a mechanism similar to silica flocculation by hydrogen-bonding polymers (*e.g.*, polyethers, polysaccharides) at acidic pH (pH < 5).[43]

To further characterize silica templating by BSA, we performed dynamic light scattering (DLS) measurements for solutions containing BSA, BSA and silicic acid, and silicic acid (at 50 °C, pH 3) and measured particle size as a function of time (Figure 4). In the presence of silicic acid (100 mM TMOS hydrolyzed in 1 mM HCl) at 50 °C, BSA molecules begin to grow at about 5 h and reach a plateau at about 16 h. Without silica and under identical conditions, BSA molecules do not change over 18 h (Figure 4). However, DLS

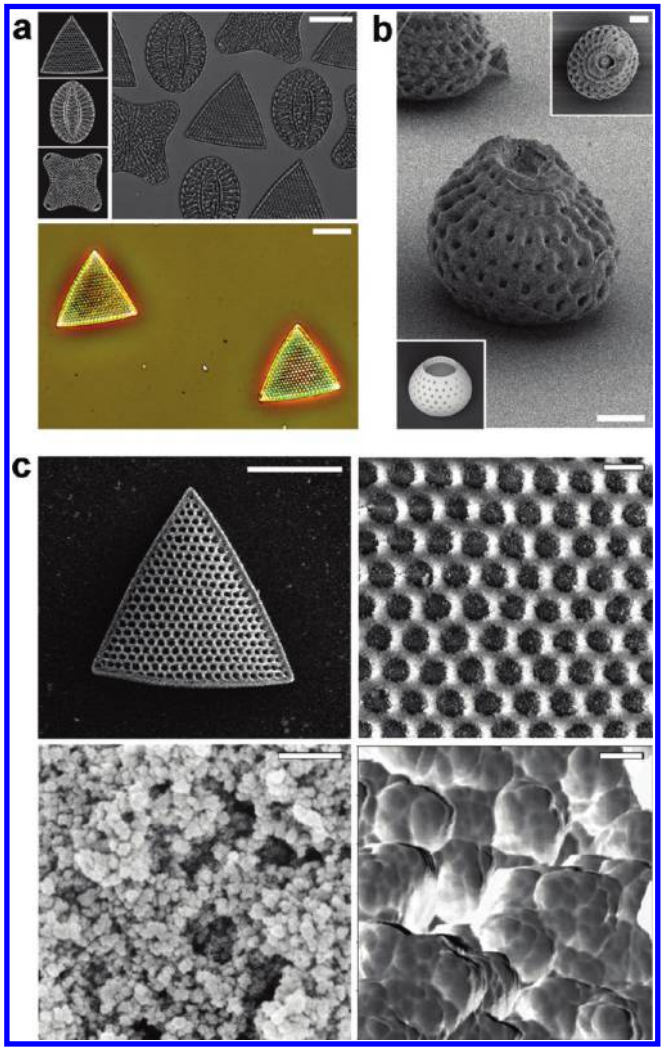

Figure 3. Microfabrication of artificial diatom and radiolarian frustules. (a) Images of diatom frustules (upper left panels) direct the fabrication of BSA protein microstructures (DIC micrograph, upper right panel; scale bar, 20 μm) using MDML; (lower panel; scale bar, 20 μm) phase micrograph of diatom-like silica microstructures. (b) CAD-designed microfabrication of artificial radiolarian frustules using MDML (scale bars, 10 μm). Upper inset shows the top view and lower inset shows a 3D rendering generated from the image sequence used to direct multiphoton fabrication. (c) Characterization of hierarchical features displayed by microfabricated diatom structures using SEM and AFM. The smallest constituent particles, on the order of ~16 nm in size, are visible in the AFM phase image, bottom right panel (scale bars clockwise from top left, 20 μm, 2 μm, 200 nm, and 50 nm).

measurements on silica sol without BSA under these conditions showed formation of 3−4 nm diameter particles after a delay of ~5 h (following the rate-limiting step of oligomer formation).[43] This particle size is consistent with the reported equilibrium size of silica particles at 50 °C.[43] The similarity of onset times for BSA growth and silica particle formation indicates that BSA most likely does not affect the kinetics of silica polymerization under these conditions but instead flocculates silica particles (≤4 nm) once they have formed.

Similar kinetics were observed for the modulus of BSA hydrogel matrices during silica condensation. Monitoring the modulus of a BSA microcantilever incubated in the pH 3 silica sol (50 °C) showed virtually no change for <3hrs. Between 3 and 8 h the modulus showed a substantial increase (Figure 4), indicating flocculation and coarsening of the silica particle network to achieve larger necked features (~16 nm) and particles (20−60 nm diameter) visible in AFM and SEM images (Figure 3b, Supporting Information, Figure S7). Similar particle sizes and features were observed by Coradin and co-workers[33] who investigated BSA-templating of silica from silicic acid at acidic pH.

With BSA acting as a flocculation determinant, the ~16 nm features observed here may indicate direct templating by individual protein molecules, corresponding to a BSA molecule in solution (a triangular shape of ~9 nm sides and ~4 nm thick)[46] coated in a 2−4 nm thick shell of silica. The protein matrix provides closely packed centers for flocculation and particle

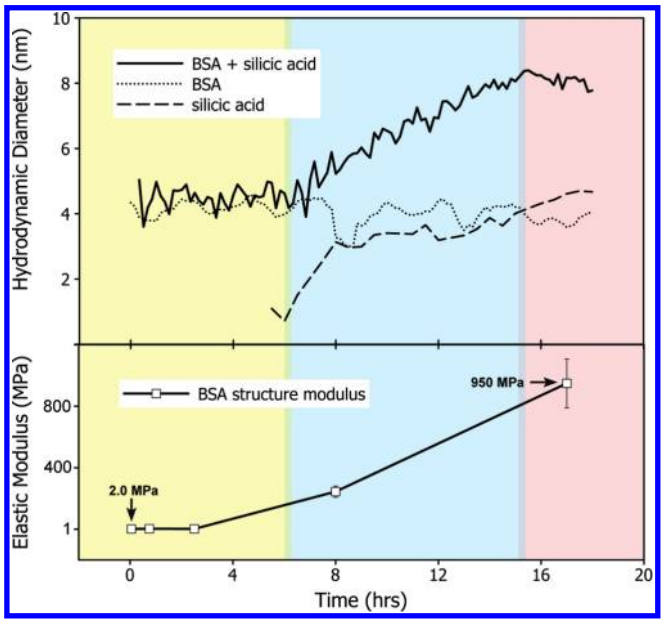

Figure 4. Time lapse characterization of particle size and microstructure modulus of silica templating by BSA. (top panel) Particle size measurements *versus* time obtained by DLS measurements of three solutions at 50 °C and pH 3 comprised of BSA and silica, BSA, and silica (solutions contained 0.1 wt % BSA and/or 100 mM TMOS). No particle growth is observed during the first hours (yellow area). Particle growth is observed over 5−16 h in BSA and silica and silica solutions (blue area), reaching a plateau for BSA and silica at ∼16 h (red area). (bottom panel) Time lapse measurement of the modulus of a BSA microcantilever incubated in 100 mM hydrolyzed TMOS, pH 3 at 50 °C. The modulus essentially remained static during the first 3 h, increasing substantially therafter. Error bars indicate 95% confidence in the mean value of the modulus. We note that for DLS measurements, the 4.5 nm hydrodynamic diameter of BSA may indicate unfolding of BSA molecules in salt-free acidic solution,[53] as we observed the expected size of 8−9 nm for BSA dissolved in PBS.

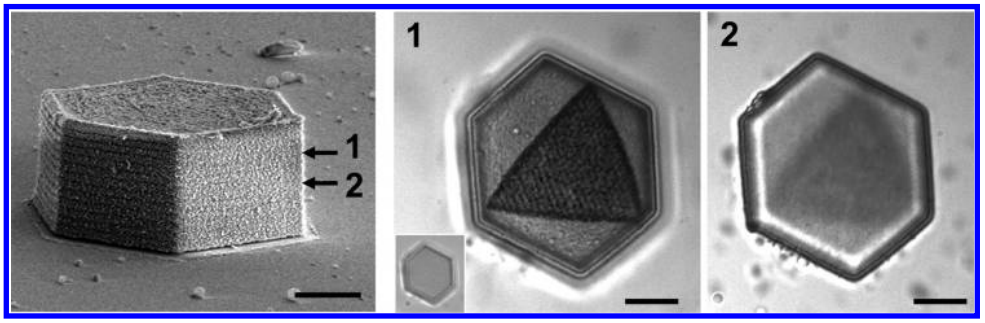

Figure 5. Photographic reproduction within a 3D porous silica hexagonal prism. BSA-templated, silica hexagonal prism containing an internal diatom-image produced *via* two-photon photoreduction of gold salts. Arrows indicate the position of DIC images in panels 1 and 2. Panel 1, lower left inset, shows the image plane before exposure to Ti:S laser light. Scale bars, 10 μm.

coarsening resulting in closely interconnected silica particles (Figure 3c, bottom left panel). Analogous to regulatory silaffins used by diatoms, incorporation of regulatory agents into the microfabricated scaffold should constrain the degrees of freedom for silica polymerization and permit assembly of precise, higher order structures/features.[1] Further, given that proteins of different identity, functional properties, and net charge (*e.g.*, BSA, avidin, and lysozyme) all form protein/silica composites under these conditions and that template removal does not alter the silica framework indicates a potential route to develop molecular (protein) imprinted materials with arbitrary microscopic shapes—for sensing and separation applications[47]—using this approach.

Finally, the nanoporosity of these structures provides opportunities for high-density functionalization in arbitrary 3D microgeometries. To demonstrate this feature, we immersed a BSA-templated, hexagonal silica prism in a solution of Au^{3+} and laser printed an image of a diatom within the structure (Figure 5) *via* multiphoton photoreduction of gold ions into nanoparticles.[48] Thickness of the image is ∼2 μm (estimated using DIC imaging) embedded ∼5 μm from the top of the structure. This provides a route to advance, for instance, information storage applications using arbitrary 3D topologies combined with 3D microprinting using both topological (*e.g.*, DVD, "blu-ray") and multilayer readout.[49] Further, metallic components can be readily integrated into functional geometries

using this approach, for example, to connect confined cell populations (Figure 2) to electrodes using direct-write leads.[50] Further work will explore these opportunities to develop, for instance, biosensors and microbial fuel cells using highly organized, 3D cell populations.

CONCLUSION

We have described a strategy to generate arbitrary 3D silica architectures *via* protein-directed silica flocculation and coarsening within a hydrogel scaffold. The key method underpinning template fabrication, MDML, can be readily extended to millimeter-length scales,[29] offering control over hierarchical features across ~7 orders of magnitude. Importantly, protein-directed assembly of silica is amenable to single-photon patterning of the protein template (Supporting Information, Figures S4 and S5 and Experimental Section), facilitating translation of this approach to standard 2D photolithographic practices. In contrast to nearly all photolithographic processes that involve chemical templating, development, and/or thermal processing procedures (*e.g.*, shrinkage of SU8[51] and direct ink writing[28] scaffolds), the use of protein hydrogel scaffolds permits high fidelity replication of the template without significant volume changes in the resulting replica (Figure 2). We further demonstrated both replication (Figure 3a and c) and design (Figure 3b) of complex diatom/radiolarian morphologies comprised of silica. The ability to design/prototype silica architectures in 3D followed by transformational chemistries, for instance silica to silicon as demonstrated here (Figure 1), should enable a wide range of complex inorganic architectures to be explored, in particular those that require precise 3D geometries (*e.g.*, photonics, bioimplants), hierarchical, high surface area features with robust mechanical properties, and that benefit from high-density functionalization (*e.g.*, sensors, catalysts).

Finally, though there has been significant progress in the past decade toward an understanding of the molecular components involved in biogenic silica formation, questions remain regarding, for example, the interaction between regulatory (*e.g.*, regulatory silaffins) and silica-condensing catalytic domains (*e.g.*, amine chains, catalytic silaffins) of the organic scaffold.[1] This is evidenced by a current inability to reproduce diatom-like silica features *in vitro* using native, silica-associated biomolecules. This work provides a foundation to address this problem, by investigating silica formation under the constraints of user-defined biotemplates on the scale of microorganisms incorporating (native, synthetic, *etc.*) regulatory, flocculating, and catalytic components.

METHODS

Protein Hydrogel Microfabrication. Microstructures composed of photo-cross-linked protein were fabricated from solutions containing protein at 200−320 mg/mL (unless otherwise specified) and methylene blue (4 mM) as a photosensitizer. Microstructure geometries were defined using a mask-directed multiphoton fabrication approach previously described in detail.[39] Briefly, protein structures were fabricated onto untreated no. 1 microscope coverslips by using the output of a mode-locked titanium:sapphire laser (Tsunami; Spectra Physics) operating at 740−750 nm, pulse width of 60 fs, and a repetition rate of 80 MHz. The laser focus was raster scanned with an X/Y open frame scan head (Nutfield Technology) across a reflectance mask (digital micromirror device) used to define the features of protein microstructures as the laser focus was stepped axially from the substrate. The laser output was adjusted by using optics to approximately fill the back aperture of an oil-immersion objective (Nikon 100× Fluar, 1.3 numerical aperture) situated on a Nikon inverted microscope. Laser power, obtained by attenuating the laser beam using a half-wave plate/polarizing beam splitter pair, measured *ca.* 30 mW at the objective.

Silicification of BSA Protein Templates and Calcination. Following fabrication, BSA microstructures were incubated in PBS (pH 7) overnight at 50 °C, which was observed to prevent template swelling in the acidic silica sol. Structures were then incubated in a 100 mM TMOS solution in 1 mM HCl (not aged) at 50 °C for 12−18 h. Silica/protein composites were dehydrated by sequential soaking in DI water, 1:1 DI water:ethanol, ethanol, 1:1 ethanol:methanol, and methanol for 10 min in each solution. Structures were then dried with filtered nitrogen gas and calcined at 500 °C for 3 h.

Magnesiothermal Reduction of Silica. Silica structures were reduced to silicon following a previously described procedure[18] with some modifications. The sample was sealed between a 1in. Swagelok brass cap and a 1in. Swagelok stainless steel plug. The brass cap has an inside fitting which undergoes expansion during heating, sealing against the stainless steel; the differing metals keep the reaction vessel from seizing. Sufficient magnesium was used to consume the O_2 and N_2 contained inside the chamber (about 25 mg). The reactor was heated for 2.5 h at 650 °C. After cooling, the sample was placed in 1 M HCl for 2 h to remove residual MgO and Si_2Mg.

Surface Area and Porosity of BSA-Templated Silica. BSA hydrogels were photochemically prepared using the $[Ru(bpy)_3]^{2+}$-mediated photochemical cross-linking of tyrosine residues.[52] A solution containing BSA (340 mg/mL), $[Ru(bpy)_3]^{2+}$ (2 mM), and ammonium persulfate (50 mM) in PBS was subjected to a high-power white-light source for 2 min. Silicification and calcination of the BSA hydrogel were performed under identical conditions, as reported in the text for multiphoton fabricated hydrogels. Nitrogen adsorption data for the BSA-templated silica was collected with a Micromeritics ASAP 2020 porosimetry analyzer, with surface area and pore size distribution calculated using BET analysis and a density functional theory model for cylindrical pores in an oxide material, respectively.

Atomic Force Microscopy (AFM). High-resolution AFM was used to characterize the silica microstructure. A commercial AFM (MFP 3D Bio, Asylum Research) with SSS-NCH cantilevers (Nanoworld, tip radius <2 nm) was used in tapping mode (free amplitude 500 mV). *In situ* measurement and analysis of material modulus are described in detail elsewhere.[41] Briefly, a tipless AFM cantilever was used to depress the microstructure cantilever and measure its deflection. Stiff TL-NCH cantilevers (Nanosensors, k = 42 N/m) were used for testing of silicificated cantilevers.

Scanning Electron Microscopy (SEM) and Energy Dispersive Spectroscopy (EDS). Protein microstructures were fixed in 2.5% gluteraldehyde solution for 20 min, dehydrated by using 10 min sequential

washes (2:1 ethanol/H2O; twice in 100% ethanol; 1:1 ethanol/methanol; 100% methanol; all solutions stated as vol/vol), allowed to air dry for 3 h, and sputter-coated to nominal thicknesses of 10 nm with Au. Images in Figures 1 and 3b were recorded using an FEI Quanta series SEM. This instrument was equipped with an EDS from EDAX which was used in multipoint mode for elemental analysis of microstructures. Images in Figure 3c were recorded using a Hitachi S-5200 SEM.

Optical Microscopy. Differential interference contrast (DIC) images (Figures 2, 3a, upper right panel, 5, right two panels) were acquired on an inverted Nikon microscope (Eclipse TI) equipped with DIC optics and using a 100× oil-immersion objective. Phase micrographs (Figure 3a, lower panel) were acquired on a Nikon Eclipse E600 equipped with phase optics and using a 20× air objective.

Dynamic Light Scattering (DLS). DLS measurements were done in a 10 mm spectroscopic cell at 90° scattering angle. The instrument was home-built using a 532 nm fiber-coupled single-frequency diode-pumped solid-state laser (approximately 20 mW at the sample) and two single-photon avalanche detector photon counters. Correlation functions were fitted with a double exponential decay for the case of BSA (bimodal distribution confirmed by CONTIN) with the faster mode attributed to the individual particles and a single exponential decay for the case of silica control sample. The hydrodynamic diameter was calculated from the particles diffusion coefficient and the Stokes−Einstein relation. The relative photon count was calculated by subtracting the signal from DI water (as well as that of BSA aggregates for the case of the protein solutions).

Photoprinting within Silica Matrices. Silica hexagonal prisms were templated using BSA. Structures were rinsed in a solution of 1 mM $AuCl_3$ and 0.05 mM rhodamine for 10 min. MDML (at similar Ti:S laser powers as used for microfabrication) was used to produce the opaque diatom image structure *via* two photon photoreduction[48] of Au^{3+}, and the solution was rinsed (five times) with water prior to DIC imaging.

Acknowledgment. We thank A. McClung for help with 3D rendering, C. Brodie for use of diatom images, and X. Jiang for help with TEM. This work was supported by the Air Force Office of Scientific Research grant 9550-10-1-0054, U.S. Department of Energy, Office of Basic Energy Sciences, Division of Materials Sciences and Engineering. B.K. gratefully acknowledges the Sandia National Laboratories Truman Fellowship in National Security Science and Engineering and the Laboratory Directed Research and Development program for support. Sandia is a multiprogram laboratory operated by Sandia Corporation, a Lockheed Martin Company, for the United States DOE's NNSA under contract DE-AC04-94AL85000.

Supporting Information Available: Modulus measurements, SEM, nitrogen sorption data, FTIR, and AFM characterization of materials. This material is available free of charge *via* the Internet at http://pubs.acs.org.

REFERENCES AND NOTES

1. Hildebrand, M. Diatoms, Biomineralization Processes, and Genomics. *Chem. Rev.* **2008,** *108*, 4855–4874.
2. Dickerson, M. B.; Sandhage, K. H.; Naik, R. R. Protein- and Peptide-Directed Syntheses of Inorganic Materials. *Chem. Rev.* **2008,** *108*, 4935–4978.
3. Gordon, R.; Losic, D.; Tiffany, M. A.; Nagy, S. S.; Sterrenburg, F. A. S. The Glass Menagerie: Diatoms for Novel Applications in Nanotechnology. *Trends Biotechnol.* **2009,** *27*, 116–127.
4. Losic, D.; Mitchell, J. G.; Voelcker, N. H. Diatomaceous Lessons in Nanotechnology and Advanced Materials. *Adv. Mater.* **2009,** *21*, 2947–2958.
5. Parker, A. R.; Townley, H. E. Biomimetics of Photonic Nanostructures. *Nat. Nanotech.* **2007,** *2*, 347–353.
6. Sanchez, C.; Arribart, H.; Guille, M. M. G. Biomimetism and Bioinspiration As Tools for the design of Innovative Materials and Systems. *Nat. Mater.* **2005,** *4*, 277–288.
7. Cha, J. N.; Shimizu, K.; Zhou, Y.; Christiansen, S. C.; Chmelka, B. F.; Stucky, G. D.; Morse, D. E. Silicatein Filaments and Subunits From a Marine Sponge Direct the Polymerization of Silica and Silicones *In vitro*. *Proc. Natl. Acad. Sci. U.S.A.* **1999,** *96*, 361–365.
8. Luckarift, H. R.; Spain, J. C.; Naik, R. R.; Stone, M. O. Enzyme Immobilization in a Biomimetic Silica Support. *Nat. Biotechnol.* **2004,** *22*, 211–213.
9. Kroger, N.; Lorenz, S.; Brunner, E.; Sumper, M. Self-assembly of Highly Phosphorylated Silaffins and Their Function in Biosilica Morphogenesis. *Science* **2002,** *298*, 584–586.
10. Groeger, C.; Lutz, K.; Brunner, E. Biomolecular Self-Assembly and Its Relevance in Silica Biomineralization. *Cell Biochem. Biophys.* **2008,** *50*, 23–39.
11. Losic, D.; Mitchell, J. G.; Voelcker, N. H. Fabrication of Gold Nanostructures by Templating from Porous Diatom Frustules. *New J. Chem.* **2006,** *30*, 908–914.
12. Losic, D.; Mitchell, J.; Lal, R.; Voelcker, N. Rapid Fabrication of Micro-and Nanoscale Patterns by Replica Molding from Diatom Biosilica. *Adv. Funct. Mater.* **2007,** *17*, 2439–2446.
13. Shian, S.; Cai, Y.; Weatherspoon, M. R.; Allan, S. M.; Sandhage, K. H. Three-Dimensional Assemblies of Zirconia Nanocrystals *via* Shape-Preserving Reactive Conversion of Diatom Microshells. *J. Am. Chem. Soc.* **2005,** *89*, 694–698.
14. Cai, Y.; Allan, S. M.; Sandhage, K. H.; Zalar, F. M. Three-Dimensional Magnesia-Based Nanocrystal Assemblies *via* Low-Temperature Magnesiothermic Reaction of Diatom Microshells. *J. Am. Chem. Soc.* **2005,** *88*, 2005–2010.
15. Unocic, R. R.; Zalar, F. M.; Sarosi, P. M.; Cai, Y.; Sandhage, K. H. Anatase Assemblies from Algae: Coupling Biological Self-assembly of 3-D Nanoparticle Structures with Synthetic Reaction Chemistry. *Chem. Commun.* **2004,** *2004*, 796–797.
16. Sandhage, K. H.; Dickerson, M. B.; Huseman, P. M.; Caranna, M. A.; Clifton, J. D.; Bull, T. A.; Heibel, T. J.; Overton, W. R.; Schoenwaelder, M. E. A. Novel, Bioclastic Route to Self-Assembled, 3D, Chemically Tailored Meso/Nanostructures: Shape-Preserving Reactive Conversion of Biosilica (Diatom) Microshells. *Adv. Mater.* **2002,** *14*, 429–433.
17. Zhao, J.; Gaddis, C. S.; Cai, Y.; Sandhage, K. H. Free-Standing Microscale Structures of Nanocrystalline Zirconia with Biologically Replicable Three-Dimensional Shapes. *J. Mater. Res.* **2005,** *20*, 282–287.
18. Bao, Z.; Weatherspoon, M. R.; Shian, S.; Cai, Y.; Graham, P. D.; Allan, S. M.; Ahmad, G.; Dickerson, M. B.; Church, B. C.; Kang, Z. Chemical Reduction of Three-Dimensional Silica Micro-Assemblies into Microporous Silicon Replicas. *Nature* **2007,** *446*, 172–175.
19. Gaddis, C. S.; Sandhage, K. H. Freestanding Microscale 3D Polymeric Structures with Biologically-Derived Shapes and Nanoscale Features. *J. Mater. Res.* **2004,** *19*, 2542.
20. Li, X.; Bian, C.; Chen, W.; He, J.; Wang, Z.; Xu, N.; Xue, G. Polyaniline on Surface Modification of Diatomite: A Novel Way to Obtain Conducting Diatomite Fillers. *Appl. Surf. Sci.* **2003,** *207*, 378–383.
21. Cai, X.; Zhu, G.; Zhang, W.; Zhao, H.; Wang, C.; Qiu, S.; Wei, Y. Diatom-Templated Synthesis of Ordered Meso/Macroporous Hierarchical Materials. *Eur. J. Inorg. Chem.* **2006,** *2006*, 3641–3645.
22. Holmes, S. M.; Graniel-Garcia, B. E.; Foran, P.; Hill, P.; Roberts, E. P. L.; Sakakini, B. H.; Newton, J. M. A Novel Porous Carbon Based on Diatomaceous Earth. *Chem. Commun.* **2006,** *2006*, 2662–2663.
23. Rosi, N. L.; Thaxton, C. S.; Mirkin, C. A. Control of Nanoparticle Assembly by Using DNA-Modified Diatom Templates. *Angew. Chem.* **2004,** *116*, 5616–5619.
24. Payne, E. K.; Rosi, N. L.; Xue, C.; Mirkin, C. A. Sacrificial Biological Templates for the Formation of Nanostructured Metallic Microshells. *Angew. Chem.* **2005,** *117*, 5192–5195.
25. Zhou, H.; Fan, T.; Li, X.; Ding, J.; Zhang, D.; Gao, Y. Bio-Inspired Bottom-Up Assembly of Diatom-Templated Ordered Porous Metal Chalcogenide Meso/Nanostructures. *Eur. J. Inorg. Chem.* **2008,** *2009*, 211–215.
26. Ford, J.; Yang, S. Directed Synthesis of Silica Nanoparticles on Micropatterned Hydrogel Templates Tethered with Poly-ethyleneimine. *Chem. Mater.* **2007,** *19*, 5570–5575.

27. Moon, J. H.; Seo, J.; Xu, Y.; Yang, S. Direct Fabrication of 3D Silica-Like Microstructures from Epoxy-Functionalized Polyhedral Oligomeric Silsesquioxane (POSS). *J. Mater. Chem.* **2009,** *19*, 4687–4691.
28. Xu, M.; Gratson, G.; Duoss, E.; Shepherd, R.; Lewis, J. Biomimetic Silicification of 3D Polyamine-Rich Scaffolds Assembled by Direct Ink Writing. *Soft Matter* **2006,** *2*, 205–209.
29. LaFratta, C. N.; Fourkas, J. T.; Baldacchini, T.; Farrer, R. A. Multiphoton Fabrication. *Angew. Chem., Int. Ed.* **2007,** *46*, 6238–6258.
30. Tétreault, N.; von Freymann, G.; Deubel, M.; Hermatschweiler, M.; Pérez Willard, F.; John, S.; Wegener, M.; Ozin, G. A. New Route to Three Dimensional Photonic Bandgap Materials: Silicon Double Inversion of Polymer Templates. *Adv. Mater.* **2006,** *18*, 457–460.
31. Kroger, N.; Deutzmann, R.; Sumper, M. Polycationic Peptides from Diatom Biosilica That Direct Silica Nanosphere Formation. *Science* **1999,** *286*, 1129–1132.
32. Morse, D. E. Silicon Biotechnology: Harnessing Biological Silica Production to Construct New Materials. *Trends Biotechnol.* **1999,** *17*, 230–232.
33. Coradin, T.; Coupé, A.; Livage, J. Interactions of Bovine Serum Albumin and Lysozyme with Sodium Silicate Solutions. *Colloids Surf., B* **2003,** *29*, 189–196.
34. Luckarift, H.; Balasubramanian, S.; Paliwal, S.; Johnson, G.; Simonian, A. Enzyme-Encapsulated Silica Monolayers for Rapid Functionalization of a Gold Surface. *Colloids Surf., B* **2007,** *58*, 28–33.
35. Gautier, C.; Abdoul-Aribi, N.; Roux, C.; Lopez, P. J.; Livage, J.; Coradin, T. Biomimetic Dual Templating of Silica by Polysaccharide/Protein Assemblies. *Colloids Surf., B* **2008,** *65*, 140–145.
36. Bassindale, A.; Taylor, P.; Abbate, V.; Brandstadt, K. Simple and Mild Preparation of Silica-Enzyme Composites from Silicic Acid Solution. *J. Mater. Chem.* **2009,** *19*, 7606–7609.
37. Brott, L. L.; Naik, R. R.; Pikas, D. J.; Kirkpatrick, S. M.; Tomlin, D. W.; Whitlock, P. W.; Clarson, S. J.; Stone, M. O. Ultrafast Holographic Nanopatterning of Biocatalytically Formed Silica. *Nature* **2001,** *413*, 291–293.
38. Kaehr, B.; Shear, J. Mask-Directed Multiphoton Lithography. *J. Am. Chem. Soc.* **2007,** *129*, 1904–1905.
39. Nielson, R.; Kaehr, B.; Shear, J. Microreplication and Design of Biological Architectures Using Dynamic-Mask Multiphoton Lithography. *Small* **2009,** *5*, 120.
40. Kaehr, B.; Allen, R.; Javier, D.; Currie, J.; Shear, J. Guiding Neuronal Development with *In situ* Microfabrication. *Proc. Natl. Acad. Sci. U.S.A.* **2004,** *101*, 16104.
41. Khripin, C. Y.; Brinker, C. J.; Kaehr, B. Mechanically Tunable Multiphoton Fabricated Protein Hydrogels Investigated Using Atomic Force Microscopy. *Soft Matter* **2010,** *6*, 2842–2848.
42. Kaehr, B.; Shear, J. Multiphoton Fabrication of Chemically Responsive Protein Hydrogels for Microactuation. *Proc. Natl. Acad. Sci. U.S.A.* **2008,** *105*, 8850.
43. Iler, R. K. *The chemistry of silica*. Wiley: New York, 1979.
44. Kaehr, B.; Shear, J. High-Throughput Design of Microfluidics Based on Directed Bacterial Motility. *Lab Chip* **2009,** *9*, 2632–2637.
45. Connell, J.; Wessel, A.; Parsek, M.; Ellington, A.; Whiteley, M.; Shear, J. Probing Prokaryotic Social Behaviors with Bacterial "Lobster Traps". *mBio*, **2010**, *1*, e00202−10.
46. Carter, D.; Ho, J. Structure of Serum Albumin. *Advances in protein chemistry* **1994,** *45*, 153.
47. Bergmann, N.; Peppas, N. Molecularly Imprinted Polymers with Specific Recognition for Macromolecules and Proteins. *Prog. Polym. Sci.* **2008,** *33*, 271–288.
48. Tanaka, T.; Kawata, S. Three-Dimensional Multilayered Optical Memory Using Two-Photon Induced Reduction of Au3+ Doped in PMMA. *IEEE Trans. Magn.* **2007,** *43*, 828–831.
49. Royon, A., Bourhis, K., Bellec, M., Papon, G., Bousquet, B., Deshayes, Y., Cardinal, T. Canioni, L., Silver Clusters Embedded in Glass as a Perennial High Capacity Optical Recording Medium. *Adv. Mater.* **2010,** *22*, 5282−5286.
50. Wu, P.; Cheng, W.; Martini, I.; Dunn, B.; Schwartz, B.; Yablonovitch, E. Two-Photon Photographic Production of Three-Dimensional Metallic Structures within a Dielectric Matrix. *Adv. Mater.* **2000,** *12*, 1438–1441.
51. Meisel, D.; Diem, M.; Deubel, M.; Pérez Willard, F.; Linden, S.; Gerthsen, D.; Busch, K.; Wegener, M. Shrinkage Precompensation of Holographic Three Dimensional Photonic Crystal Templates. *Adv. Mater.* **2006,** *18*, 2964–2968.
52. Fancy, D.; Kodadek, T. Chemistry for the Analysis of Protein−Protein Interactions: Rapid and Efficient Cross-Linking Triggered by Long Wavelength Light. *Proc. Natl. Acad. Sci. U.S.A.* **1999,** *96*, 6020.
53. Yamasaki, M.; Yano Koichiro, H. Differential Scanning Calorimetric Studies on Bovine Serum Albumin: I. Effects of pH and Ionic Strength. *Int. J. Biol. Macromol.* **1990,** *12*, 263–268.